Advanced Glycation End-Products Suppress Mitochondrial Function and Proliferative Capacity of Achilles Tendon-Derived Fibroblasts

Shivam H. Patel[1]
Feng Yue[2]
Shannon K. Saw[1]
Rachel Foguth[3,4]
Jason R. Cannon[3,4]
Jonathan H. Shannahan[3]
Shihuan Kuang[2]
Arman Sabbaghi[5]
Chad C. Carroll[1,6*]

[1]Department of Health and Kinesiology, Purdue University, West Lafayette, IN
[2]Department of Animal Sciences, Purdue University, West Lafayette, IN
[3]School of Health Sciences, Purdue University, West Lafayette, IN
[4]Purdue Institute for Integrative Neuroscience, West Lafayette, IN
[5]Department of Statistics, Purdue University, West Lafayette, IN
[6]Indiana Center for Musculoskeletal Health, Indiana University School of Medicine, Indianapolis, IN

Running Head: AGEs and mitochondrial function in tendon fibroblasts

Keywords: tendon, diabetes, advanced glycation end-products, mitochondria, proliferation

*Address for correspondence:

Chad C. Carroll, PhD
Assistant Professor
Purdue University
Department of Health and Kinesiology
800 W. Stadium Ave
West Lafayette, IN 47907
Phone: (765) 496-6002
carrol71@purdue.edu

Abstract

Debilitating cases of tendon pain and degeneration affect the majority of diabetic individuals. The high rate of tendon degeneration persists even when glucose levels are well controlled, suggesting that other mechanisms may drive tendon degeneration in diabetic patients. The purpose of this study was to investigate the impact of advanced glycation end-products on tendon fibroblasts to further our mechanistic understanding of the development and progression of diabetic tendinopathy. We proposed that advanced glycation end-products would induce limitations to mitochondrial function and proliferative capacity in tendon-derived fibroblasts, restricting their ability to maintain biosynthesis of tendon extracellular matrix. Using an *in-vitro* cell culture system, rat Achilles tendon fibroblasts were treated with glycolaldehyde-derived advanced glycation end-products (0, 50, 100, and 200μg/ml) for 48 hours in normal glucose (5.5mM) and high glucose (25mM) conditions. We demonstrate that tendon fibroblasts treated with advanced glycation end-products display reduced ATP production, electron transport efficiency, and proliferative capacity. These impairments were coupled with alterations in mitochondrial DNA content and expression of genes associated with extracellular matrix remodeling, mitochondrial energy metabolism, and apoptosis. Our findings suggest that advanced glycation end-products disrupt tendon fibroblast homeostasis and may be involved in the development and progression of diabetic tendinopathy.

Introduction

Over 30 million Americans suffer from diabetes. Evaluation of this patient population suggests that tendon abnormalities (i.e., tendinopathies) such as collagen fibril disorganization, increased tissue stiffness, and tissue degeneration are present in the majority of diabetic individuals[1-3]. Notably, the high rate of tendinopathies in diabetic individuals persists even when glucose levels are well controlled (hemoglobin A1c<7)[2,4,5]. Given the high prevalence of diabetic tendinopathy, there is a critical need to define the molecular process underlying the diabetic tendon phenotype.

Advanced glycation end-product (AGE) formation is a non-enzymatic process in which free amine terminals are subjected to covalent modification by reactive glucose or other carbonyl containing molecules. AGEs form at an accelerated rate in diabetes and these modifications can result in non-enzymatic cross-links in long-lived extracellular proteins such as tendon collagen, which increase tissue stiffness and alter tissue mechanical properties[6-10]. Furthermore, circulating AGE adducts are able to interact with the receptor for advanced glycation end-products (RAGE) to initiate a noxious feed forward cycle of sustained inflammation and tissue damage[11]. In other tissues, endogenous AGE formation as result of chronic hyperglycemia and spontaneous oxidation of glycolytic intermediates contribute significantly to elevated levels of bound and circulating AGE adducts in diabetic patients[12,13]. Additionally, AGE-rich diets can increase serum AGE levels and result in accumulation of AGEs in tendon of mice[14]. It is not known, however, what role circulating AGEs play in the development and progression of diabetic tendinopathy.

In non-tendon models, AGEs have been shown to activate RAGE-mediated cellular pathways leading to impairments in mitochondrial function and apoptosis[15-18]. To our knowledge, the impact of AGEs on tenocyte mitochondrial function (e.g., ATP production and electron transport efficiency) has not previously been evaluated. Specifically, ATP has been shown to promote biosynthesis of the extracellular matrix (ECM) in intervertebral cells[19]. In diabetic tendinopathy, degeneration and loss of organization in the ECM may be driven, in part, by the imbalance of energy (ATP) demand and supply. We propose that AGEs contribute to the diabetic tendon phenotype by activating cellular pathways that limit mitochondrial function, thereby interfering with the capacity of tendon fibroblasts to maintain biosynthesis of tendon ECM.

In effort to better understand diabetes associated tendon pathology, we sought to characterize impairments to energy producing systems and proliferative capacity of tendon-derived fibroblasts in response to AGE treatment and high glucose containing medium. We hypothesized that AGEs, *in-vitro*, would impair mitochondrial function and proliferative capacity, independent of glucose concentrations. Further, we hypothesized that AGEs and high glucose medium would reduce mitochondrial DNA (mtDNA) content and further contribute to limitations imposed to energy producing pathways in tendon fibroblasts. To advance our understanding of mitochondrial biogenesis and energy production during AGE exposure, analysis of mitochondrial apoptotic regulators, as well as regulators of mitochondrial energy metabolism was completed. This study provides new functional and descriptive perspective of the AGE insult on tendon fibroblast homeostasis.

Results

Proliferative Capacity: Cell proliferation (EdU), cell counts, Mybl2 mRNA, Pcna mRNA, and cytostatic MTT were significantly reduced at AGE-50µg/ml, AGE-100µg/ml, and AGE-200µg/ml compared to AGE-0µg/ml ($p<0.0125$, Figure 1b-f, respectively). The HG condition had no effect on cell proliferation (EdU), cell counts, and Mybl2 mRNA ($p>0.0125$, Figure 1b-d, respectively). However, the HG condition reduced Pcna mRNA transcript counts ($p<0.0125$, Figure 1e) and increased absorbance values of cytostatic MTT data ($p<0.0125$, Figure 1f).

Mitochondrial Stress Tests: ATP production-coupled respiration was significantly reduced at AGE-100µg/ml and AGE-200µg/ml compared to AGE-0µg/ml ($p<0.0125$, Figure 2a). ATP production-coupled respiration was also significantly reduced in the HG condition ($p<0.0125$, Figure 2a). Basal respiration was significantly reduced at AGE-100µg/ml and AGE-200µg/ml compared to AGE-0µg/ml ($p<0.0125$, Figure 2b), but no glucose effect was observed ($p>0.0125$, Figure 2b). Neither AGE treatment nor glucose condition had a significant effect on maximal respiration ($p>0.0125$, Figure 2c). AGE treatment had no effect on proton leak ($p>0.0125$, Figure 2d), but the HG condition increased proton leak across the inner mitochondrial membrane ($p<0.0125$, Figure 2d). Coupling efficiency was significantly reduced at AGE-200µg/ml compared to AGE-0µg/ml ($p<0.0125$, Figure 2e). Coupling efficiency was also significantly reduced in the HG condition ($p<0.0125$, Figure 2e). Spare respiratory capacity was significantly increased at AGE-200µg/ml compared to AGE-0µg/ml ($p<0.0125$, Figure 2f), but no glucose effect was observed ($p>0.0125$, Figure 2f).

Transcriptional Analysis of Extracellular Matrix Remodeling: Col1a1 and MMP9 mRNA transcript counts were significantly reduced in the AGE-200µg/ml compared to AGE-0µg/ml ($p<0.0125$, Figure 3a&d). Col3a1 mRNA transcript counts were significantly increased in the AGE-50µg/ml and AGE-100µg/ml groups compared to AGE-0µg/ml ($p<0.0125$, Figure 3b). MMP2 mRNA transcript counts were significantly increased in the AGE-100µg/ml compared to AGE-0µg/ml ($p<0.0125$, Figure 3c). AGEs had no effect on TIMP1 mRNA transcript counts ($p<0.0125$, Figure 3e). No glucose effect was observed for Col1a1, Col3a1, MMP2, MMP9, or TIMP1 ($0<0.0125$, Figure 3a-e).

Mitochondrial DNA Content: mtDNA content was significantly increased at AGE-50µg/ml, AGE-100µg/ml, and AGE-200µg/ml compared to AGE-0µg/ml ($p<0.0125$, Figure 4a), but no effect of glucose condition was observed ($p>0.0125$, Figure 4a). Neither AGE treatment nor glucose condition had a significant effect on DNA content when normalized to cell counts ($p>0.0125$, Figure 4b).

Transcriptional Analysis of Mitochondrial Complexes: Ndufa1 mRNA transcript counts were significantly increased at AGE-50µg/ml, AGE-100µg/ml, and AGE-200µg/ml compared to AGE-0µg/ml ($p<0.0125$, Figure 5a), but no effect of glucose condition was observed ($p>0.0125$, Figure 5a). Sdha mRNA transcript counts were significantly reduced at AGE-200µg/ml compared to AGE-0µg/ml ($p<0.0125$, Figure 5b), but no effect of glucose was observed ($p>0.0125$, Figure 5b). A secondary direct comparison to test the conditional main effect revealed that Sdha transcript counts were significantly reduced at HG AGE-200µg/ml compared to HG AGE-0µg/ml ($p<0.05$, Figure 5b). Bcs1l mRNA was significantly reduced at AGE-50µg/ml, AGE-100µg/ml,

and AGE-200µg/ml compared to AGE-0µg/ml ($p<0.0125$, Figure 5c). Bcs1l mRNA was also significantly reduced in the HG condition ($p<0.0125$, Figure 5c). Neither AGE treatment nor glucose condition altered Cox4i1 mRNA transcript counts ($p>0.0125$, Figure 5d). MT-ATP6 mRNA transcript counts were significantly reduced at HG AGE-200µg/ml compared to HG AGE-0µg/ml ($p<0.05$, Figure 5e), but no effect of glucose was observed ($p>0.0125$, Figure 5e).

Protein Analysis of Mitochondrial Complexes: Expression of complex III (UQCRC2) was significantly increased at AGE-200µg/ml compared to AGE-0µg/ml ($p<0.017$, Figure 6c), but no glucose effect was observed ($p>0.017$, Figure 6c). Expression of complex I (NDUFB8), II (SDHB), IV (MTCO1), or V (ATP5A) were not altered by either AGE treatment or glucose condition ($p>0.017$, Figure 6a, b, d, & e, respectively). However, a significant interaction between AGE treatment and glucose condition was observed for complex I (NDUFB8) and complex IV (MTCO1) ($p<0.017$, Figure 6a&d).

Transcriptional Analysis of Mitochondrial Apoptosis: Bak1 mRNA transcript counts were significantly reduced at AGE-100µg/ml and AGE-200µg/ml compared to AGE-0µg/ml ($p<0.0125$, Figure 7a), but no effect of glucose condition was observed ($p>0.0125$, Figure 7a). Bax and Casp8 mRNA transcript counts were significantly reduced at HG AGE-200µg/ml compared to HG AGE-0µg/ml ($p<0.05$, Figure 7b&e, respectively), but no effect of glucose was observed ($p>0.0125$, Figure 7b&e, respectively). Bcl2 and Tgfbr3 mRNA transcript counts were significantly reduced at AGE-200µg/ml compared to AGE-0µg/ml ($p<0.0125$, Figure 7c&f, respectively), but no effect of glucose condition was observed ($p>0.0125$, Figure 7c&f, respectively). AGE

132 treatment had no effect on Casp3 mRNA ($p>0.0125$, Figure 7d), but the HG condition

133 reduced Casp3 mRNA transcript counts ($p<0.0125$, Figure 7d).

134 *Superoxide Production:* Superoxide production was significantly increased at

135 AGE-200µg/ml compared to AGE-0µg/ml ($p<0.017$, Figure 8), but no glucose effect was

136 observed ($p>0.017$, Figure 8).

Discussion

AGE-induced non-enzymatic collagen cross-link formation in the ECM has been proposed to increase tendon stiffness in diabetic individuals[6,7,10]. However, factors contributing to tendon degeneration and collagen fibril disorganization in diabetic tendon have not been extensively characterized. The detrimental effects of AGE associated pathology are well described in non-tendon tissues and have been linked to several diabetic complications such as cardiomyopathy, retinopathy, nephropathy, and endothelial dysfunction[10,20]. In this study, we sought to address the effect of AGEs at the cellular level to better understand factors that may contribute to the disorganization and degeneration of tendon ECM noted in diabetic individuals. Using an *in-vitro* primary cell culture system, we demonstrate dose-dependent AGE-induced reductions in proliferative capacity and mitochondrial ATP production of tendon-derived fibroblasts. Additionally, we demonstrate increased mtDNA content and modifications to mitochondrial complexes and markers of apoptosis after AGE treatment. While previous research has established AGE dependent mitochondrial and proliferative limitations[17,18,21], these data, to the best of our knowledge, are the first to show these impairments in tendon-derived fibroblasts.

Tendon injuries and degenerative pathology are a common and debilitating clinical problem in diabetic individuals[2,3,22-26]. Diabetic tendons are thicker[24,27], and more commonly present with fibril disorganization[2]. Despite convincing epidemiological data, the molecular factors contributing to the development and degenerative process of tendinopathy in diabetic individuals are not well characterized. Much focus has been directed to the influence of elevated glucose on cellular and structural tendon parameters. *In-vitro* and *in-vivo* data has indicated that elevated glucose availability can alter cell

160 signaling dynamics and structural properties in tendon[28-30]. These data suggest that
161 glucose may contribute to tendon pathology, however conflicting reports exist and more
162 conclusive human data is needed to confirm hyperglycemia-associated tendon
163 degeneration in diabetes.

164 As evidenced, glucose does seem to be implicated in modulation of some tendon
165 cellular and structural properties[28-30], however, the underlying mechanisms influencing
166 tendon degeneration in diabetic patients remain inconclusive. Couppé *et al.*[4] have
167 demonstrated that Achilles tendon Young's modulus (stiffness) is greater in diabetic
168 subjects compared to control subjects, but no difference exists between subjects with
169 well-controlled and poorly controlled diabetes. These data highlight that hyperglycemia
170 is unlikely to be the sole contributor of diabetic tendon pathology. In support of this
171 notion, we explored the role of AGEs on modulation of tendon cellular properties that
172 may consequently interfere with regulation and maintenance of the ECM.

173 Tendon fibroblast proliferation is a vital component to tendon development,
174 adaptation, and healing[31,32]. An inability of tenocytes to proliferate in the presence of
175 AGEs would significantly precipitate the development of tendinopathy[38]. Tendinopathy is
176 thought to develop, in part, from a failed healing response to minor tendon damage
177 during loading. Specifically, delayed and abnormal healing is a common complication of
178 both type I and type II diabetes[33,34]. As evidence, tendinopathies in diabetic patients are
179 generally more pervasive and can present with more severe degeneration, which may, in
180 part, be driven by prolonged injury status[2,35,36]. We note dramatic impairments to tendon
181 fibroblast proliferative capacity in the presence of AGEs. Our *in-vitro* data demonstrate,
182 in a dose dependent fashion, reduced cell proliferation (EdU) and cell counts after 48

hours of AGE treatment (Figure 1b&c, respectively). In concert, we demonstrate a reduction in proliferative gene markers, Mybl2 and Pcna, and reduced absorbance values of cytostatic MTT with AGE treatment (Figure 1d-f, respectively). These data are in agreement with data from Hu *et al*.[21], which also demonstrates a lack of proliferative capacity in the presence of AGEs. While the HG condition did impact Pcna mRNA and cytostatic MTT (Figure 1e-f), the primary insult to proliferative capacity appears to be driven by AGE treatment. Impaired proliferation is likely mediated by RAGE signaling[37], but further work is needed to confirm AGE-mediated impairments to tendon fibroblast proliferation and tendon healing.

AGEs have been linked to numerous diabetes related complications and their detrimental effects are well documented in several tissues[10,20]. The primary consequences of AGE-mediated RAGE activation are chronic inflammation, as result of the NF-κB mediated cascade, and oxidative stress, due to NADPH oxidase stimulation. Among resulting complications, reports in other cell types have identified AGE-mediated impairments to mitochondrial function and dynamics[15-18]. Similarly, we report impaired mitochondrial parameters and reduced ATP production-coupled respiration in tendon fibroblasts treated with AGEs (Figure 2a). The role of ATP is diverse and essential for a multitude of cellular processes including cell proliferation, contraction, and wound healing. Specifically, ATP has been shown to promote biosynthesis of the ECM in intervertebral disk cells[19]. In tendon, the resident fibroblast population maintains the ECM, which is primarily composed of collagen. Due to the energy demanding nature of ECM maintenance, it is possible, that in the presence of AGEs, limited ATP production contributes to loss of organization in the ECM, which is commonly noted in diabetic

206 tendon[1-3]. While maximal respiration of tendon fibroblasts was unchanged due to
207 identical XFp seeding density, basal respiration was reduced after AGE treatment (Figure
208 2b&c, respectively). In addition to loss of ATP production and reduced basal respiration,
209 we demonstrate that AGEs also impair electron transport coupling efficiency; thereby
210 increasing spare respiratory capacity of AGE treated tendon fibroblasts and indicating
211 overall reduction to electron transport efficiency (Figure 2e&f, respectively).
212 Interestingly, the HG condition increased proton leak across the inner mitochondrial
213 membrane and reduced ATP production and coupling efficiency, suggesting that glucose
214 alone can also impact electron transport efficiency (Figure 2d). It is important to note that
215 AGE and/or glucose-mediated mitochondrial impairments are likely not the sole
216 contributor of tendon ECM disorganization. For example, AGEs increase matrix
217 metalloproteinases (MMP) expression and activity, which may contribute in an additive
218 manner to enhanced degeneration in tendon ECM[38].
219 To address our hypothesis that the presence of AGEs and resulting limited ATP
220 production contribute to loss of organization in the ECM, we completed gene analysis of
221 targets associated with ECM maintenance and remodeling. We note that AGE treatment
222 reduces Col1a1 mRNA expression (Figure 3a), consistent with previous work which has
223 demonstrated reduced collagen synthesis during AGE treatment in fibroblasts[39]. Col3a1
224 mRNA expression was however increased with AGE 50µg/ml and 100µg/ml, but not at
225 200µg/ml (Figure 3b). Col3a1 expression is upregulated after injury and during the early
226 stages of wound healing[40,41]. It is possible that in our cell culture model, increased Col3a1
227 mRNA expression in the AGE 50µg/ml and 100µg/ml groups was an attempt to
228 overcome the AGE insult to tendon fibroblast collagen production. However, it appears

229 that the potential compensatory response was unsuccessful in the AGE 200μg/ml group
230 (Figure 3b). Further, MMPs and tissue inhibitors of metalloproteinases (TIMPs) work to
231 tightly regulate remodeling of ECM remodeling. Previous work in chondrocyte cell
232 culture has demonstrated an increase to MMP mRNA expression with AGE
233 treatment[42,43]. While we did observe increased MMP2 mRNA expression in the AGE
234 100μg/ml group, MMP9 mRNA expression was reduced in the AGE 200μg/ml group
235 (Figure 3c&d). Lastly, we did not observe an AGE or glucose effect of TIMP1 mRNA
236 (Figure 3e. Reduced collagen expression and altered MMP modulation may favor an
237 environment that promotes loss of ECM organization. Future work evaluating post-
238 translational MMP activation and collagen fibril organization is needed to determine the
239 role of AGEs in modulation of tendon ECM.

240 We also noted increased content of mtDNA after 48 hours of AGE treatment,
241 despite striking reductions to ATP production. mtDNA content can be used as an estimate
242 of mitochondrial volume[44], however, contrary to our hypothesis, 48 hours of AGE
243 treatment resulted in increased mtDNA content in a dose dependent manner independent
244 of glucose condition (Figure 4a). Based on our findings, it is plausible that the increase in
245 mtDNA in AGE-treated tendon fibroblasts was indicative of a compensatory response to
246 overcome the AGE insult and meet energy demands[45,46]. In support of this theory, cells
247 under oxidative stress have been shown to increase mitochondria and mtDNA[47].
248 Additionally, Kim *et al*.[46] have demonstrated a relationship between mtDNA content and
249 severity of histopathology in cancerous lesions, suggesting that increased mtDNA content
250 may be used as a measure of DNA injury and pathology. Despite this compensatory
251 response, functional mitochondrial limitations were still evident after 48 hours of AGE

252 treatment. Alternatively, it is possible that AGE-induced limitations to mitochondrial
253 biogenesis may result in failure of tendon fibroblasts to meet energy demands. For
254 example, mtDNA is more susceptible to mutation than nuclear DNA and AGEs have
255 been shown to induce damage to mtDNA, which could ultimately impact mitochondrial
256 biogenesis[48,49]. However, further molecular work is needed to conclusively define the
257 pathway of AGE-mediated mitochondrial damage. To confirm that mtDNA content
258 measurements were not falsely elevated by an increase in total DNA, despite equal DNA
259 loading per PCR reaction, we normalized total DNA yield to cell counts and noted no
260 difference in DNA content with either glucose condition or AGE treatment (Figure 4b).
261 Reactive oxygen species (ROS), produced primarily by mitochondria, have been
262 implicated in AGE-mediated cell apoptosis and mitochondrial damage[18,50,51]. To further
263 explore and identify specific targets of the AGE insult, we assessed regulation of electron
264 transport complexes and apoptosis. Analysis of gene transcripts associated with complex
265 I-V (Figure 5a-e, respectively) of the electron transport chain revealed increased
266 expression of Ndufa1 mRNA (Figure 5a) and marked reduction of Bcs1l mRNA (Figure
267 5c) with AGE treatment. Additionally, the HG condition further reduced Bcs1l mRNA
268 expression (Figure 5c). Increased Ndufa1 mRNA after AGE treatment may be interpreted
269 as a compensatory response to increase mitochondrial complex I in effort to meet energy
270 demands after the AGE insult. However, Bcs1l mRNA, which encodes mitochondrial
271 complex III, is dramatically reduced in a dose dependent manner after AGE treatment,
272 suggesting that the AGE insult may be targeted to complex III. Lastly, Sdha and MT-
273 ATP6 mRNA, coding for mitochondrial complex II and complex V (ATP synthase),
274 respectively, were reduced in the HG AGE-200μg/ml group compared to HG AGE-

0µg/ml (Figure 5b&e, respectively). A direct comparison was made between HG AGE-0µg/ml and HG AGE-200µg/ml to test the conditional main effect and reveal a significant reduction to Sdha and MT-ATP6 mRNA, suggesting that both AGE treatment and HG condition were contributing to this reduction. Cox4i1 (complex IV, Figure 5d) was not impacted by either AGE treatment or HG condition. While these gene data provide indication that AGEs may indeed have targeted effects to the electron transport chain, protein analysis revealed only complex III (UQCRC2) to be affected by an AGE main effect (Figure 6c). Additionally, complex III protein expression was increased with AGE exposure, while complex III mRNA expression was reduced. Lack of response to remaining complexes and discrepancies between gene and protein analysis may be attributed to the acute duration of AGE exposure. Further, an interaction between AGEs and glucose condition was observed in complex I (NDUFB8, Figure 6a) and complex IV (MTCO1, Figure 6d). These results merit further work to discover mechanistic pathways by which AGEs limit mitochondrial function during long-term AGE exposure.

To assess the impact of AGEs on mitochondrial-related tendon fibroblast apoptosis, we completed analysis of associated gene transcripts and measurement of superoxide production. Transcript counts of pro-apoptotic gene Bak1 were reduced with AGE treatment (Figure 7a). Additionally, pro-apoptotic Bax mRNA expression was reduced only in the HG AGE-200µg/ml group compared to HG AGE-0µg/ml (Figure 7b). Although these findings are contrary to previous work[21], it is possible that these may be compensatory responses to AGE-mediated apoptotic signals. In agreement with previous work by Hu *et al*.[21], expression of Bcl2 mRNA, an anti-apoptotic mediator, was reduced with AGE treatment (Figure 7c). Previous reports have indicated an inverse relationship

between Bcl2 and ROS, where ROS may act to reduce expression of Bcl2 and sensitize cells to apoptosis[52]. In agreement, our data demonstrate increased production of superoxide, a reactive anion species, after AGE treatment (Figure 8). Further, cytochrome c release is suppressed by Bcl2, but is promoted by Bak1 and Bax. Cytochrome c release will ultimately result in caspase activation[53]. Previous reports indicate AGE treatment induces caspase activation[21,54], however we did not note any AGE-induced changes to Casp3 mRNA (Figure 7d) but did note reduced Casp8 mRNA in the HG AGE-200μg/ml group compared to HG AGE-0μg/ml (Figure 7e). Finally, transcript counts of Tgfbr3 were reduced with AGE treatment (Figure 7f). Tgfbr3 overexpression has been shown to increase Bax and Bcl2 expression, as well as promote activation of caspase 3[55]. Casp3 mRNA expression was reduced in the HG condition and was the only target associated with apoptosis to be affected by glucose (Figure 7d). From these data, it is evident that AGEs alter transcriptional regulation of gene transcripts associated with apoptosis, however, we are limited in our interpretation and further post-translational and activity assays are needed to define the precise mechanisms by which AGEs may induce apoptosis in diabetic tendinopathy.

In summary (Figure 9), we demonstrate that AGEs, which are elevated in serum of diabetic individuals, impair proliferative capacity, ATP production, and electron transport chain efficiency. Additionally we demonstrate that AGEs alter regulation of mitochondrial complex expression and gene transcripts associated with apoptosis. While the HG condition did impact some mitochondrial parameters, AGEs appear to be the primary insult and may be responsible for the development of the diabetic tendon phenotype. This work provides new insights to the pathophysiology of tendon ECM in

321 diabetic patients. However, future *in-vivo* and mechanistic work is needed to determine

322 whether controlling serum AGEs in diabetic patients can reduce risk of degenerative

323 tendinopathy.

Methods

AGE Preparation: Glycolaldehyde-derived AGEs were generated under sterile conditions as described by Valencia *et al.*[56]. Briefly, sterile filtered 30% BSA solution (Sigma, St. Louis, MO) was incubated with 70mM glycolaldehyde dimer (Sigma) in sterile PBS without calcium chloride and magnesium chloride for three days at 37°C. After incubation, the AGE product was dialyzed against sterile PBS for 24 hours at 4°C using gamma-irradiated 10kDa cut-off cassettes (Thermo Scientific, Waltham, MA) to remove unreacted glycolaldehyde. Unmodified control BSA was prepared similarly, without the addition of glycolaldehyde dimer. Protein concentration was determined by BCA assay (Thermo Scientific) and absence of endotoxin (<0.25Eu/ml) was confirmed via the LAL gel-clot assay (GenScript, Piscataway, NJ).

Extent of AGE Modification: Extent of BSA modification was confirmed by fluorescence, absorbance, and loss of primary amines[56-59]. AGE-BSA and Control-BSA were diluted to 1mg/ml in PBS and fluorescent spectra and absorbance were recorded at 335nm excitation/420nm emission and 340nm, respectively (Molecular Devices, San Jose, CA). For determination of loss of primary amines AGE-BSA and Control-BSA were diluted to 0.2mg/ml in PBS. An equal volume of ortho-phthalaldehyde solution (Sigma) was added and fluorescent spectrum was recorded at 340nm excitation/455nm emission (Molecular Devices). A standard curve of 0 to 0.2mg/ml of BSA that did not undergo 37°C incubation was used to generate a standard curve of free amine content and data was normalized to represent percentage of amine terminals remaining with reference to the standard curve[56]. Respective fluorescence or absorbance values of PBS alone were subtracted from all data. AGE-BSA fluorescence was increased to 697.78 arbitrary units

(AU) compared to -0.72 AU for control BSA. Absorbance readings were completed to determine the extent of glycation. AGE-BSA showed increased glycation with absorbance readings of 0.682 AU compared to 0.01 AU for control BSA. Finally, AGE-BSA primary amine terminals underwent complete modification (-0.03% accessible amine terminals remaining), while control BSA retained 81.48% of accessible amine terminals. Spectra and absorbance values of PBS alone were subtracted from data but resulted in negative values for fluorescent-based detection because the spectra of PBS alone was greater than the obtained sample values. Negative values were interpreted as zero, and extent of modification was similar to previous reports[56].

Animal Protocol: This study was approved by the Purdue University Institutional Animal Care and Use Committee and all animals were cared for in accordance with the recommendations in the Guide for the Care and Use of Laboratory Animals[60]. Eight-week-old female Sprague-Dawley rats (n=8, 256.43±5.19g) were purchased from Charles River Laboratories (Wilmington, MA) and maintained for an additional eight weeks. Rats were housed on a 12-hour light-dark cycle and provided access to standard rat chow and water ad libitum. At sixteen weeks, rats were euthanized by decapitation after CO_2 inhalation.

Tendon Fibroblast Isolation and Cell Culture: Tendon-derived fibroblasts were isolated from the Achilles tendons of eight rats. After euthanasia, Achilles tendons were carefully excised and trimmed of remaining muscle and fascia. The tendon was rinsed with sterile PBS, finely minced, placed in DMEM containing 0.2% type I collagenase, and incubated in a 37°C shaking water bath for four hours. After tissue digestion, the cell suspension was filtered through a 100μm mesh filter, pelleted by centrifugation, resuspended in 5.5mM glucose DMEM containing 10% FBS, 1% sodium pyruvate

(Sigma), and 1% penicillin/streptomycin (Thermo Scientific) and plated in 100mm collagen coated dishes. After reaching ~75-80% confluence, tendon fibroblasts were subcultured with either normal glucose (NG, 5.5mM) DMEM (Sigma) or high glucose (HG, 25mM) DMEM (Sigma) for a minimum of one passage to allow for glucose condition acclimation. Tendon fibroblasts were then seeded into 6-well, 24-well, or 96-well collagen coated culture plates and treated for 48 hours with 0, 50, 100, and 200µg/ml of AGEs within both glucose conditions. The 0µg/ml AGE group was treated with 200µg/ml of unmodified control BSA. Tendon fibroblasts from passage 2-4 were used for all experiments.

Proliferative Capacity: Proliferative capacity was assessed by cell counts, cytostatic MTT, and incorporation of synthetic nucleoside 5-ethynyl-2´-deoxyuridine (EdU). After AGE treatment in 6-well plates, cells were enzymatically released and manually counted with a hemocytometer. Cell counts were completed in duplicate and normalized to total volume in which cells were resuspended. For cytostatic MTT analysis, cells cultured in a 96-well plate were incubated with MTT reagent (5mg/ml, VWR, Radnor, PA) for the final 90 minutes of AGE treatment. Formazan crystals were solubilized with DMSO and absorbance was read at 550nm (Multiskan, Thermo Scientific). Each assay was completed in duplicate and data was represented as absolute arbitrary absorbance units. Cells were labeled with 2.5µM EdU (Carbosynth, Newbury, UK) during the final 12 hours of AGE treatment. EdU is a thymidine analog that incorporates during active DNA synthesis and is used to mark proliferating cells. Fixed cells (4% PFA) were stained with DAPI, and EdU was visualized via the Click-iT method (100mM Tris-HCl pH8.5, 1mM $CuSO_4$, 2.5µM red-fluorescent

tetramethylrhodamine azide, and 100mM ascorbic acid; Thermo Scientific)[61]. Fluorescent images were captured using a DMI 6000B microscope (Leica, Wetzlar, Germany) with a 10x objective and MetaMorph software (Molecular Devices). EdU data was analyzed using the ImageJ Multi-Point Tool (National Institutes of Health, Bethesda, Maryland) and is reported as a ratio of EdU^+ nuclei to total nuclei from two fields-of-view within each treatment.

Mitochondrial Stress Tests: Tendon fibroblasts were treated for 48 hours prior to being plated (8,000 cells) into collagen coated XFp cell culture miniplates (Seahorse Bioscience, Agilent, Santa Clara, CA). Cultured cells from each treatment condition were reseeded in duplicate, allowed to attach to the miniplates, and washed twice in pre-warmed XF base medium (Agilent). Miniplates were then incubated in XF base medium (1mM sodium pyruvate, 2mM glutamine, and either 5.5mM or 25mM glucose) for one hour in a 37°C incubator without CO_2 to allow plate outgassing. Mitochondrial stress experiments were completed on an XFp extracellular flux analyzer (Agilent) with the Mito Stress Test Kit (Agilent). Chemicals (1µM oligomycin, 0.5µM carbonyl cyanide-*4*-(trifluoromethoxy)phenylhydrazone (FCCP), 0.5µM rotenone, and 0.5µM antimycinA) were preloaded into cartridge ports and injected in succession during measurement of oxygen consumption rate (OCR).

Gene Expression Analysis: Total RNA for gene expression analysis was isolated after AGE treatment using the Direct-zol RNA Miniprep kit (Zymo Research). On-column DNase digestion was completed on all samples prior to elution of RNA. RNA concentration was determined using a NanoDrop 2000 (Thermo Scientific). Quality of RNA was assessed using the 260/280 and 260/230 ratios. Reverse transcription (iScript,

BioRad) was completed to produce complementary DNA from 100ng of RNA. Absolute quantification of mRNA target transcripts was completed using the ddPCR platform (BioRad) with validated probe-based assays (BioRad) as previously described[30]. For optimal detection, Col1a1 and Col3a1 reactions contained 0.55ng of cDNA, while MMP2, MMP9, and TIMP1 contained 4.4ng of cDNA[30]. All other target PCR reactions contained 2.2ng of cDNA. A list of measured gene targets is provided in Table 1.

Mitochondrial DNA Content: mtDNA content was quantified by ratio of a target mitochondrial gene, NADH dehydrogenase subunit 1 (ND1), to nuclear reference gene, protein argonaute-1 (EIF2C1)[62,63]. Total DNA was isolated using the Quick-DNA Microprep kit (Zymo Research, Irvine, CA). DNA concentration was determined using a NanoDrop 2000 (Thermo Scientific) and serial diluted to 1ng/µl. A droplet digital PCR (ddPCR) method was used to complete quantification of absolute copy number of both ND1 and EIF2C1. Reactions were prepared in duplex format, in a final volume of 20µl with 2x ddPCR Supermix for Probes (No dUTP) (BioRad, Hercules, CA), 20x reference probe ND1 labeled with FAM (BioRad), 20x reference probe EIF2C1 labeled with HEX (BioRad), 5ng of DNA, 1µl of HindIII enzyme (FastDigest, Thermo Scientific), and nuclease-free water. The assembled reaction was incubated at room temperature for 20 minutes to permit digestion with the HindIII restriction enzyme. After digestion, droplets were generated from prepared PCR reactions using Droplet Generation Oil for Probes (BioRad) on a QX200 Droplet Generator (BioRad), transferred to a deep-well 96-well plate, and amplified (95°C-10 minutes, 1 cycle; 94°C-30 seconds and 60°C-90 seconds, 40 cycles; 98°C-10 minutes, 1 cycle) on a C1000 thermal cycler (BioRad). At completion of end-point PCR, absolute quantification of PCR products was completed on a QX200

Droplet Reader (BioRad) with QuantaSoft Software Version 1.7 (BioRad) and reported as a ratio of positive ND1/EIF2C1 counts per 20µl reaction.

Protein Expression: Cultured cells were lysed in RIPA buffer containing 50mM Tris-HCl, 150mM NaCl, 2mM EDTA, 2mM EGTA, 0.5% sodium deoxycholate, 1% Triton X-100, 0.1% SDS, 50mM NaF, 0.2mM Na_3VO_4, and 0.2% protease inhibitor cocktail (Sigma). Samples were prepared as described previously[64]. Equal amounts of protein (15µg) were separated in duplicate on an Any-kD TGX polyacrylamide gel (BioRad). Protein was transferred to a PVDF membrane (TransBlot Turbo, BioRad) and blocked for 24 hours at 4°C in 5% blotting-grade blocker (BioRad). Blots were incubated in primary OXPHOS antibody (1:1000, 110413, Abcam, Cambridge, MA) and then HRP-conjugated goat anti-mouse antibody (1:5000, 31430, Invitrogen), each for 2 hours at room temperature. Bands of interest were compared against positive control (Rat Heart Mitochondria, Abcam) and all targets were probed on the same membrane, but required different exposure times using signal accumulation mode (ChemiDoc, BioRad). Volume intensity analysis of matched exposure duration for each target was completed using Image Lab Version 6.0.1 (BioRad). Total protein volume intensity obtained by UV activated Stain-Free imaging was used for data normalization.

Superoxide Production: Superoxide (O_2^-) production was determined by dihydroethidium (DHE) derived fluorescence. Cultured cells were detached, pelleted, and resuspended in Hank's Balanced Salt Solution. An aliquot was saved for determination of cell concentration. DHE (Thermo Scientific) was added at final concentration of 10µM and samples were incubated with shaking at 37°C for 30 minutes[65-67]. Fluorescent

spectrum was recorded at 530nm excitation/590nm emission (Molecular Devices) and fluorescence units were normalized to cell concentration.

Statistical Analysis: Statistical analyses on the four main effect contrasts of interest (50μg/ml AGE vs. 0μg/ml AGE, 100μg/ml AGE vs. 0μg/ml AGE, 200μg/ml AGE vs. 0μg/ml AGE, and HG vs. LG) for each outcome variable proceeded via a mixed effects regression model with consideration of technical data replicates and random effects to account for the tendon fibroblast donor rats. Regression models were fit to the data using the `lmer` function in `R`. The Kenward-Roger F-test was performed to determine whether the main effects regression model or the "full" model containing both main effects and two-factor interactions between the AGE and glucose contrasts should be fitted. Validity of the assumptions for the models were assessed via standard regression diagnostics. Specifically, the standardized residuals were examined to assess whether they were approximately Normally distributed, centered at zero, and did not exhibit any patterns with respect to the predictor variables. If assumptions appeared invalid for the original scale, the logarithmic and square root transformations were considered. After identifying a model that provided a good fit to the outcome data, hypothesis tests were performed for the contrasts using Satterthwaite's method, and confidence intervals were created using the bootstrap. Hypothesis tests for the contrasts use a Bonferroni-adjusted significance level of $\alpha=0.05/4=0.0125$ (Figures 1-5 and 7) or $\alpha=0.05/3=0.017$ (Figures 6 and 8) separately across the different outcome variables to account for the multiple comparisons. Certain specified, direct comparisons between two specific groups were performed via the paired t-test in `R` with $\alpha=0.05$ to test conditional main effects, where HG was conditioned for testing the AGE contrast of interest.

Summary of applied contrasts and exact p-values for significant findings are provided in Table 2. Figures were generated in Prism 7.0 (GraphPad, La Jolla, CA) and are represented as mean ± standard error.

References

1 Abate, M., Salini, V. & Schiavone, C. Achilles tendinopathy in elderly subjects with type II diabetes: the role of sport activities. *Aging clinical and experimental research* **28**, 355-358, doi:10.1007/s40520-015-0391-7 (2016).

2 Batista, F. *et al.* Achilles tendinopathy in diabetes mellitus. *Foot Ankle Int* **29**, 498-501, doi:968803 [pii] 10.3113/FAI.2008.0498 (2008).

3 Grant, W. P. *et al.* Electron microscopic investigation of the effects of diabetes mellitus on the Achilles tendon. *J Foot Ankle Surg* **36**, 272-278; discussion 330 (1997).

4 Couppe, C. *et al.* Human Achilles tendon glycation and function in diabetes. *Journal of applied physiology* **120**, 130-137, doi:10.1152/japplphysiol.00547.2015 (2016).

5 Lin, T. T. *et al.* The effect of diabetes, hyperlipidemia, and statins on the development of rotator cuff disease: a nationwide, 11-year, longitudinal, population-based follow-up study. *Am J Sports Med* **43**, 2126-2132, doi:10.1177/0363546515588173 (2015).

6 Eriksen, C. *et al.* Systemic stiffening of mouse tail tendon is related to dietary advanced glycation end products but not high-fat diet or cholesterol. *Journal of applied physiology* **117**, 840-847, doi:10.1152/japplphysiol.00584.2014 (2014).

7 Monnier, V. M. *et al.* Cross-linking of the extracellular matrix by the maillard reaction in aging and diabetes: an update on "a puzzle nearing resolution". *Annals of the New York Academy of Sciences* **1043**, 533-544, doi:10.1196/annals.1333.061 (2005).

8 Reddy, G. K., Stehno-Bittel, L. & Enwemeka, C. S. Glycation-induced matrix stability in the rabbit achilles tendon. *Archives of biochemistry and biophysics* **399**, 174-180, doi:10.1006/abbi.2001.2747 (2002).

9 Reddy, G. K. Cross-linking in collagen by nonenzymatic glycation increases the matrix stiffness in rabbit achilles tendon. *Experimental diabesity research* **5**, 143-153, doi:10.1080/15438600490277860 (2004).

10 Singh, V. P., Bali, A., Singh, N. & Jaggi, A. S. Advanced glycation end products and diabetic complications. *The Korean journal of physiology & pharmacology : official journal of the Korean Physiological Society and the Korean Society of Pharmacology* **18**, 1-14, doi:10.4196/kjpp.2014.18.1.1 (2014).

11 Kierdorf, K. & Fritz, G. RAGE regulation and signaling in inflammation and beyond. *Journal of leukocyte biology* **94**, 55-68, doi:10.1189/jlb.1012519 (2013).

12 Brownlee, M. Biochemistry and molecular cell biology of diabetic complications. *Nature* **414**, 813-820, doi:10.1038/414813a (2001).

13 Giardino, I., Edelstein, D. & Brownlee, M. Nonenzymatic glycosylation in vitro and in bovine endothelial cells alters basic fibroblast growth factor activity. A model for intracellular glycosylation in diabetes. *The Journal of clinical investigation* **94**, 110-117, doi:10.1172/jci117296 (1994).

14 Skovgaard, D. *et al.* An advanced glycation endproduct (AGE)-rich diet promotes accumulation of AGEs in Achilles tendon. *Physiological reports* **5**, doi:10.14814/phy2.13215 (2017).

15 Nelson, M. B. *et al.* Cardiomyocyte mitochondrial respiration is reduced by receptor for advanced glycation end-product signaling in a ceramide-dependent manner. *American journal of physiology. Heart and circulatory physiology* **309**, H63-69, doi:10.1152/ajpheart.00043.2015 (2015).

16 Coughlan, M. T. *et al.* Advanced glycation end products are direct modulators of beta-cell function. *Diabetes* **60**, 2523-2532, doi:10.2337/db10-1033 (2011).

17 Lo, M. C. *et al.* Nepsilon-(carboxymethyl) lysine-induced mitochondrial fission and mitophagy cause decreased insulin secretion from beta-cells. *American journal of physiology. Endocrinology and metabolism* **309**, E829-839, doi:10.1152/ajpendo.00151.2015 (2015).

18 Mao, Y. X. *et al.* RAGE-dependent mitochondria pathway: a novel target of silibinin against apoptosis of osteoblastic cells induced by advanced glycation end products. *Cell death & disease* **9**, 674, doi:10.1038/s41419-018-0718-3 (2018).

19 Gonzales, S., Wang, C., Levene, H., Cheung, H. S. & Huang, C. C. ATP promotes extracellular matrix biosynthesis of intervertebral disc cells. *Cell and tissue research* **359**, 635-642, doi:10.1007/s00441-014-2042-2 (2015).

20 Tan, K. C. *et al.* Advanced glycation end products and endothelial dysfunction in type 2 diabetes. *Diabetes Care* **25**, 1055-1059 (2002).

21 Hu, Y. *et al.* Mitochondrial Pathway Is Involved in Advanced Glycation End Products-Induced Apoptosis of Rabbit Annulus Fibrosus Cells. *Spine*, doi:10.1097/brs.0000000000002930 (2018).

22 Guney, A. *et al.* Biomechanical properties of Achilles tendon in diabetic vs. non-diabetic patients. *Exp Clin Endocrinol Diabetes* **123**, 428-432, doi:10.1055/s-0035-1549889 (2015).

23 James, V. J., Delbridge, L., McLennan, S. V. & Yue, D. K. Use of X-ray diffraction in study of human diabetic and aging collagen. *Diabetes* **40**, 391-394 (1991).

24 Abate, M., Schiavone, C. & Salini, V. Sonographic evaluation of the shoulder in asymptomatic elderly subjects with diabetes. *BMC musculoskeletal disorders* **11**, 278, doi:10.1186/1471-2474-11-278 (2010).

25 Bedi, A. *et al.* Diabetes mellitus impairs tendon-bone healing after rotator cuff repair. *Journal of shoulder and elbow surgery* **19**, 978-988, doi:10.1016/j.jse.2009.11.045 (2010).

26 Fox, A. J. *et al.* Diabetes mellitus alters the mechanical properties of the native tendon in an experimental rat model. *Journal of orthopaedic research : official publication of the Orthopaedic Research Society* **29**, 880-885, doi:10.1002/jor.21327 (2011).

27 de Oliveira, R. R. *et al.* Experimental diabetes induces structural, inflammatory and vascular changes of Achilles tendons. *PloS one* **8**, e74942, doi:10.1371/journal.pone.0074942 (2013).

28 Wu, Y. F. *et al.* High glucose alters tendon homeostasis through downregulation of the AMPK/Egr1 pathway. *Scientific reports* **7**, 44199, doi:10.1038/srep44199 (2017).

29 Tsai, W. C. *et al.* High glucose concentration up-regulates the expression of matrix metalloproteinase-9 and -13 in tendon cells. *BMC musculoskeletal disorders* **14**, 255, doi:10.1186/1471-2474-14-255 (2013).

30 Patel, S. H., Sabbaghi, A. & Carroll, C. C. Streptozotocin-induced diabetes alters transcription of multiple genes necessary for extracellular matrix remodeling in rat patellar tendon. *Connective tissue research*, 1-11, doi:10.1080/03008207.2018.1470168 (2018).

31 Yang, G., Rothrauff, B. B. & Tuan, R. S. Tendon and ligament regeneration and repair: clinical relevance and developmental paradigm. *Birth defects research. Part C, Embryo today : reviews* **99**, 203-222, doi:10.1002/bdrc.21041 (2013).

32 Thomopoulos, S., Parks, W. C., Rifkin, D. B. & Derwin, K. A. Mechanisms of tendon injury and repair. *Journal of orthopaedic research : official publication of the Orthopaedic Research Society* **33**, 832-839, doi:10.1002/jor.22806 (2015).

33 Ahmed, A. S. Does Diabetes Mellitus Affect Tendon Healing? *Advances in experimental medicine and biology* **920**, 179-184, doi:10.1007/978-3-319-33943-6_16 (2016).

34 Ahmed, A. S. *et al.* Type 2 diabetes impairs tendon repair after injury in a rat model. *J Appl Physiol* **113**, 1784-1791, doi:10.1152/japplphysiol.00767.2012 (2012).

35 Abate, M., Schiavone, C., Salini, V. & Andia, I. Occurrence of tendon pathologies in metabolic disorders. *Rheumatology (Oxford)* **52**, 599-608, doi:10.1093/rheumatology/kes395 (2013).

36 Lui, P. P. Y. Tendinopathy in diabetes mellitus patients-Epidemiology, pathogenesis, and management. *Scand J Med Sci Sports* **27**, 776-787, doi:10.1111/sms.12824 (2017).

37 Li, G., Xu, J. & Li, Z. Receptor for advanced glycation end products inhibits proliferation in osteoblast through suppression of Wnt, PI3K and ERK signaling. *Biochemical and biophysical research communications* **423**, 684-689, doi:10.1016/j.bbrc.2012.06.015 (2012).

38 Killian, M. L. & Thomopoulos, S. Scleraxis is required for the development of a functional tendon enthesis. *Faseb j* **30**, 301-311, doi:10.1096/fj.14-258236 (2016).

39 Owen, W. F., Jr. *et al.* Beta 2-microglobulin modified with advanced glycation end products modulates collagen synthesis by human fibroblasts. *Kidney international* **53**, 1365-1373, doi:10.1046/j.1523-1755.1998.00882.x (1998).

40 Merkel, J. R., DiPaolo, B. R., Hallock, G. G. & Rice, D. C. Type I and type III collagen content of healing wounds in fetal and adult rats. *Proceedings of the Society for Experimental Biology and Medicine. Society for Experimental Biology and Medicine (New York, N.Y.)* **187**, 493-497 (1988).

41 Hurme, T., Kalimo, H., Sandberg, M., Lehto, M. & Vuorio, E. Localization of type I and III collagen and fibronectin production in injured gastrocnemius muscle. *Laboratory investigation; a journal of technical methods and pathology* **64**, 76-84 (1991).

42 Nah, S. S. *et al.* Advanced glycation end products increases matrix metalloproteinase-1, -3, and -13, and TNF-alpha in human osteoarthritic chondrocytes. *FEBS letters* **581**, 1928-1932, doi:10.1016/j.febslet.2007.03.090 (2007).

43 Li, W. *et al.* Effect of advanced glycation end products, extracellular matrix metalloproteinase inducer and matrix metalloproteinases on type-I collagen metabolism. *Biomedical reports* **4**, 691-693, doi:10.3892/br.2016.641 (2016).

44 Menshikova, E. V. *et al.* Effects of exercise on mitochondrial content and function in aging human skeletal muscle. *The journals of gerontology. Series A, Biological sciences and medical sciences* **61**, 534-540 (2006).

45 Shigenaga, M. K., Hagen, T. M. & Ames, B. N. Oxidative damage and mitochondrial decay in aging. *Proceedings of the National Academy of Sciences of the United States of America* **91**, 10771-10778 (1994).

46 Kim, M. M. *et al.* Mitochondrial DNA quantity increases with histopathologic grade in premalignant and malignant head and neck lesions. *Clinical cancer research : an official journal of the American Association for Cancer Research* **10**, 8512-8515, doi:10.1158/1078-0432.ccr-04-0734 (2004).

47 Lee, H. C., Yin, P. H., Lu, C. Y., Chi, C. W. & Wei, Y. H. Increase of mitochondria and mitochondrial DNA in response to oxidative stress in human cells. *The Biochemical journal* **348 Pt 2**, 425-432 (2000).

48 Pun, P. B. & Murphy, M. P. Pathological significance of mitochondrial glycation. *International journal of cell biology* **2012**, 843505, doi:10.1155/2012/843505 (2012).

49 Cline, S. D. Mitochondrial DNA damage and its consequences for mitochondrial gene expression. *Biochimica et biophysica acta* **1819**, 979-991, doi:10.1016/j.bbagrm.2012.06.002 (2012).

50 Ott, M., Gogvadze, V., Orrenius, S. & Zhivotovsky, B. Mitochondria, oxidative stress and cell death. *Apoptosis : an international journal on programmed cell death* **12**, 913-922, doi:10.1007/s10495-007-0756-2 (2007).

51 Sifuentes-Franco, S., Pacheco-Moises, F. P., Rodriguez-Carrizalez, A. D. & Miranda-Diaz, A. G. The Role of Oxidative Stress, Mitochondrial Function, and Autophagy in Diabetic Polyneuropathy. *Journal of diabetes research* **2017**, 1673081, doi:10.1155/2017/1673081 (2017).

52 Hildeman, D. A. *et al.* Control of Bcl-2 expression by reactive oxygen species. *Proceedings of the National Academy of Sciences of the United States of America* **100**, 15035-15040, doi:10.1073/pnas.1936213100 (2003).

53 Jiang, X. & Wang, X. Cytochrome C-mediated apoptosis. *Annu Rev Biochem* **73**, 87-106, doi:10.1146/annurev.biochem.73.011303.073706 (2004).

54 Wang, Z. *et al.* Effect of advanced glycosylation end products on apoptosis in human adipose tissue-derived stem cells in vitro. *Cell & bioscience* **5**, 3, doi:10.1186/2045-3701-5-3 (2015).

55 Zheng, F. *et al.* Transient overexpression of TGFBR3 induces apoptosis in human nasopharyngeal carcinoma CNE-2Z cells. *Bioscience reports* **33**, e00029, doi:10.1042/bsr20120047 (2013).

56 Valencia, J. V. *et al.* Advanced glycation end product ligands for the receptor for advanced glycation end products: biochemical characterization and formation kinetics. *Analytical biochemistry* **324**, 68-78 (2004).

57 Westwood, M. E. & Thornalley, P. J. Molecular characteristics of methylglyoxal-modified bovine and human serum albumins. Comparison with glucose-derived advanced glycation endproduct-modified serum albumins. *Journal of protein chemistry* **14**, 359-372 (1995).

58 Verzijl, N. *et al.* Age-related accumulation of Maillard reaction products in human articular cartilage collagen. *The Biochemical journal* **350 Pt 2**, 381-387 (2000).

59 Monnier, V. M., Kohn, R. R. & Cerami, A. Accelerated age-related browning of human collagen in diabetes mellitus. *Proceedings of the National Academy of Sciences of the United States of America* **81**, 583-587 (1984).

60 Council, N. R. *Guide for the Care and Use of Laboratory Animals*. 8th edn, (The National Academies Press, 2011).

61 Salic, A. & Mitchison, T. J. A chemical method for fast and sensitive detection of DNA synthesis in vivo. *Proceedings of the National Academy of Sciences of the United States of America* **105**, 2415-2420, doi:10.1073/pnas.0712168105 (2008).

62 Li, B. *et al.* Droplet digital PCR shows the D-Loop to be an error prone locus for mitochondrial DNA copy number determination. *Scientific reports* **8**, 11392, doi:10.1038/s41598-018-29621-1 (2018).

63 Memon, A. A. *et al.* Quantification of mitochondrial DNA copy number in suspected cancer patients by a well optimized ddPCR method. *Biomolecular detection and quantification* **13**, 32-39, doi:10.1016/j.bdq.2017.08.001 (2017).

64 Patel, S. H. *et al.* Impact of acetaminophen consumption and resistance exercise on extracellular matrix gene expression in human skeletal muscle. *Am J Physiol Regul Integr Comp Physiol* **313**, R44-r50, doi:10.1152/ajpregu.00019.2017 (2017).

65 Kawase, M. *et al.* Exacerbation of delayed cell injury after transient global ischemia in mutant mice with CuZn superoxide dismutase deficiency. *Stroke* **30**, 1962-1968 (1999).

66 Nazarewicz, R. R., Bikineyeva, A. & Dikalov, S. I. Rapid and specific measurements of superoxide using fluorescence spectroscopy. *Journal of biomolecular screening* **18**, 498-503, doi:10.1177/1087057112468765 (2013).

67 Hildeman, D. A. *et al.* Reactive oxygen species regulate activation-induced T cell apoptosis. *Immunity* **10**, 735-744 (1999).

Acknowledgements

This work was supported by NIH pre-doctoral fellowship F31-AR073647 (SHP) and Purdue University Research Initiative Funds (CCC). The authors would like to acknowledge Zachary Hettinger, MS, Christopher Kargl, MS, and Sukhmani Kaur for technical laboratory assistance.

Author Contributions

S.H.P and C.C.C conceived and designed the study. S.H.P, F.Y, S.K.S, R.F, A.S, and C.C.C performed data collection and analysis. S.H.P, F.Y, S.K.S, R.F, J.R.C, J.H.S, S.K, A.S, and C.C.C interpreted data and provided expert advice. S.H.P and C.C.C drafted the manuscript. All authors edited, revised, read, and approved the final submitted manuscript.

Competing Interests

The authors declare no competing interests.

Data Availability

C.C.C has access to all data and data is available upon request.

712 **Figure Legend**

713

714 **Figure 1:** Proliferative Capacity (n=8). **a.** Representative images of EdU^+/DAPI overlay
715 after 48 hours of AGE treatment. EdU^+ nuclei are pink and have active DNA synthesis.
716 Blue nuclei (DAPI) do not have active DNA synthesis. **b.** Graphical representation of
717 EdU images (Panel A). Data represented as ratio of EdU^+ nuclei to total nuclei. **c.** Cell
718 counts after 48 hours of AGE treatment. Dashed line represents initial seeding density of
719 15,000 cells. **d&e.** ddPCR gene transcript counts for Myb-related protein B (Mybl2) and
720 proliferating cell nuclear antigen (Pcna). **f.** Cytostatic MTT shown as absolute arbitrary
721 absorbance units. *$p<0.0125$ main effect for AGE vs. AGE-0μg/ml, mixed effects
722 regression. NG:HG $p<0.0125$ indicates main effect for glucose condition, mixed effects
723 regression. Data presented as mean ± standard error. ■ Normal Glucose (NG), ■ High
724 Glucose (HG).

725

726 **Figure 2:** Mitochondrial Stress Tests (n=8). **a-f.** Mitochondrial parameters as a function
727 of oxygen consumption rate (OCR). *$p<0.0125$ main effect for AGE vs. AGE-0μg/ml,
728 mixed effects regression. NG:HG $p<0.0125$ indicates main effect for glucose condition,
729 mixed effects regression. Data presented as mean ± standard error. ■ Normal Glucose
730 (NG), ■ High Glucose (HG).

731

732 **Figure 3:** Transcriptional Analysis of Extracellular Matrix Remodeling (n=4). **a-e.**
733 ddPCR gene transcript counts for Collagen alpha-1(I) chain (Col1a1), Collagen alpha-
734 1(III) chain (Col3a1), Matrix metallopeptidase 2 (MMP2), Matrix metalloproteinase 9

(Col3a1), and Tissue inhibitor of matrix metalloproteinase 1 (TIMP1).*p<0.0125 main effect for AGE vs. AGE-0µg/ml, mixed effects regression. Data presented as mean ± standard error. ■ Normal Glucose (NG), ■ High Glucose (HG).

Figure 4: Mitochondrial DNA Content (n=8). **a.** mtDNA content quantified by ratio of mitochondrial gene, NADH dehydrogenase subunit 1 (ND1), to nuclear reference gene, protein argonaute-1 (EIF2C1). **b.** Total DNA content normalized to cell counts. *p<0.0125 main effect for AGE vs. AGE-0µg/ml, mixed effects regression. Data presented as mean ± standard error. ■ Normal Glucose (NG), ■ High Glucose (HG).

Figure 5: Transcriptional Analysis of Mitochondrial Complexes (n=8). **a-e.** ddPCR gene transcript counts for NADH:ubiquinone oxidoreductase subunit A1 (Ndufa1), Succinate dehydrogenase complex flavoprotein subunit A (Sdha), BCS1 homolog, ubiquinol-cytochrome c reductase complex chaperone (Bcs1l), Cytochrome c oxidase subunit 4i1 (Cox4i1), and ATP synthase 6, mitochondrial (MT-ATP6). *p<0.0125 main effect for AGE vs. AGE-0µg/ml, mixed effects regression. †p<0.05 vs. HG AGE-0µg/ml, paired t-test. NG:HG p<0.0125 indicates main effect for glucose condition, mixed effects regression. Data presented as mean ± standard error. ■ Normal Glucose (NG), ■ High Glucose (HG).

Figure 6: Protein Analysis of Mitochondrial Complexes (n=4). **a-e**. OXPHOS protein expression for mitochondrial complex I (NDUFB8), complex II (SDHB), complex III (UQCRC2), complex IV (MTCO1), and complex V (ATP5A). F. Representative blot

758 images (displayed in order of molecular weight) including Stain Free (SF) UV visualized
759 total protein. All targets were probed on the same membrane, but are cropped due to
760 different exposure times required for each target (Signal Accumulation Mode). *p<0.017
761 main effect for AGE vs. AGE-0µg/ml, mixed effects regression. Interaction p<0.017,
762 significant interaction between AGE treatment and glucose condition. Data presented as
763 mean ± standard error. ■ Normal Glucose (NG), ■ High Glucose (HG).
764
765 **Figure 7:** Transcriptional Analysis of Mitochondrial Apoptosis (n=8). **a-f.** ddPCR gene
766 transcript counts for BCL2-antagonist/killer 1 (Bak1), BCL2 associated X, apoptosis
767 regulator (Bax), B-cell lymphoma 2, apoptosis regulator (Bcl2), Caspase 3 (Casp3),
768 Caspase 8 (Casp8), and Transforming growth factor beta receptor 3 (Tgfbr3). *p<0.0125
769 main effect for AGE vs. AGE-0µg/ml, mixed effects regression. †p<0.05 vs. HG AGE-
770 0µg/ml, paired t-test. NG:HG p<0.0125 indicates main effect for glucose condition,
771 mixed effects regression. Data presented as mean ± standard error. ■ Normal Glucose
772 (NG), ■ High Glucose (HG).
773
774
775 **Figure 8:** Superoxide Production (n=4). *p<0.017 main effect for AGE vs. AGE-0µg/ml,
776 mixed effects regression. Data presented as mean ± standard error. ■ Normal Glucose
777 (NG), ■ High Glucose (HG).
778
779 **Figure 9:** Summary of Major AGE-Mediated Findings. Figure created with BioRender.

Table 1: ddPCR Gene Targets

Gene Symbol	Description	Gene ID
Bak1	BCL2-antagonist/killer 1	116502
Bax	BCL2 associated X, apoptosis regulator	24887
Bcl2	B-cell lymphoma 2, apoptosis regulator	24224
Bcs1l	BCS1 homolog, ubiquinol-cytochrome c reductase complex chaperone	301514
Casp3	Caspase 3	25402
Casp8	Caspase 8	64044
Col1a1	Collagen alpha-1(I) chain	29393
Col3a1	Collagen alpha-1(III) chain	84032
Cox4i1	Cytochrome c oxidase subunit 4i1	29445
MMP2	Matrix metallopeptidase 2	81686
MMP9	Matrix metalloproteinase 9	84687
MT-ATP6	ATP synthase 6, mitochondrial	26197
Mybl2	MYB proto-oncogene like 2	296344
Ndufa1	NADH:ubiquinone oxidoreductase subunit A1	363441
Pcna	Proliferating cell nuclear antigen	25737
Sdha	Succinate dehydrogenase complex flavoprotein subunit A	157074
Tfgbr3	Transforming growth factor beta receptor 3	29610
TIMP1	Tissue inhibitor of matrix metalloproteinase 1	116510

Table 2: Summary of p-values for Statistical Findings

Figure	AGE-0µg/ml vs. AGE-50µg/ml	AGE-0µg/ml vs. AGE-100µg/ml	AGE-0µg/ml vs. AGE-200µg/ml	Normal vs. High Glucose	Interaction
1B	$4x10^{-5}$	$3x10^{-14}$	$< 2x10^{-16}$	NS	N/A
1C	$1x10^{-8}$	$5x10^{-15}$	$< 2x10^{-16}$	NS	N/A
1D	$1.5x10^{-10}$	$< 2x10^{-16}$	$< 2x10^{-16}$	NS	N/A
1E	$4x10^{-9}$	$2x10^{-15}$	$< 2x10^{-16}$	$7x10^{-3}$	N/A
1F	$5x10^{-9}$	$1.5x10^{-14}$	$< 2x10^{-16}$	$8x10^{-4}$	N/A
2A	NS	$3x10^{-7}$	$2x10^{-14}$	$1x10^{-3}$	N/A
2B	NS	$9x10^{-6}$	$5x10^{-10}$	NS	N/A
2C	NS	NS	NS	NS	N/A
2D	NS	NS	NS	$2x10^{-3}$	N/A
2E	NS	NS	$1x10^{-14}$	$1x10^{-7}$	N/A
2F	NS	NS	$3x10^{-4}$	NS	N/A
3A	NS	NS	$5x10^{-11}$	NS	N/A
3B	$5x10^{-4}$	$1.4x10^{-5}$	NS	NS	N/A
3C	NS	$3x10^{-4}$	NS	NS	N/A
3D	NS	NS	$7x10^{-3}$	NS	N/A
3E	NS	NS	NS	NS	N/A
4A	$6x10^{-7}$	$1x10^{-12}$	$2x10^{-15}$	NS	N/A
4B	NS	NS	NS	NS	N/A
5A	$6x10^{-6}$	$8x10^{-7}$	7x10-5	NS	N/A
5B	NS	NS	5x10-3	NS	N/A
5C	$2x10^{-5}$	$1x10^{-11}$	$< 2x10^{-16}$	$1x10^{-2}$	N/A
5D	NS	NS	NS	NS	N/A
5E	NS	NS	NS	NS	N/A
6A	N/A	N/A	NS	NS	$1.2x10^{-2}$
6B	N/A	N/A	NS	NS	NS
6C	N/A	N/A	$1.3x10^{-2}$	NS	NS
6D	N/A	N/A	NS	NS	$2.8x10^{-3}$
6E	N/A	N/A	NS	NS	NS
7A	NS	$9x10^{-7}$	$< 2x10^{-16}$	NS	N/A
7B	NS	NS	NS	NS	N/A
7C	NS	NS	$7x10^{-10}$	NS	N/A
7D	NS	NS	NS	$1.1x10^{-2}$	N/A
7E	NS	NS	NS	NS	N/A
7F	NS	NS	$1x10^{-4}$	NS	N/A
8	N/A	N/A	$8.6x10^{-3}$	NS	NS

NS = Not Significant N/A = Not Tested

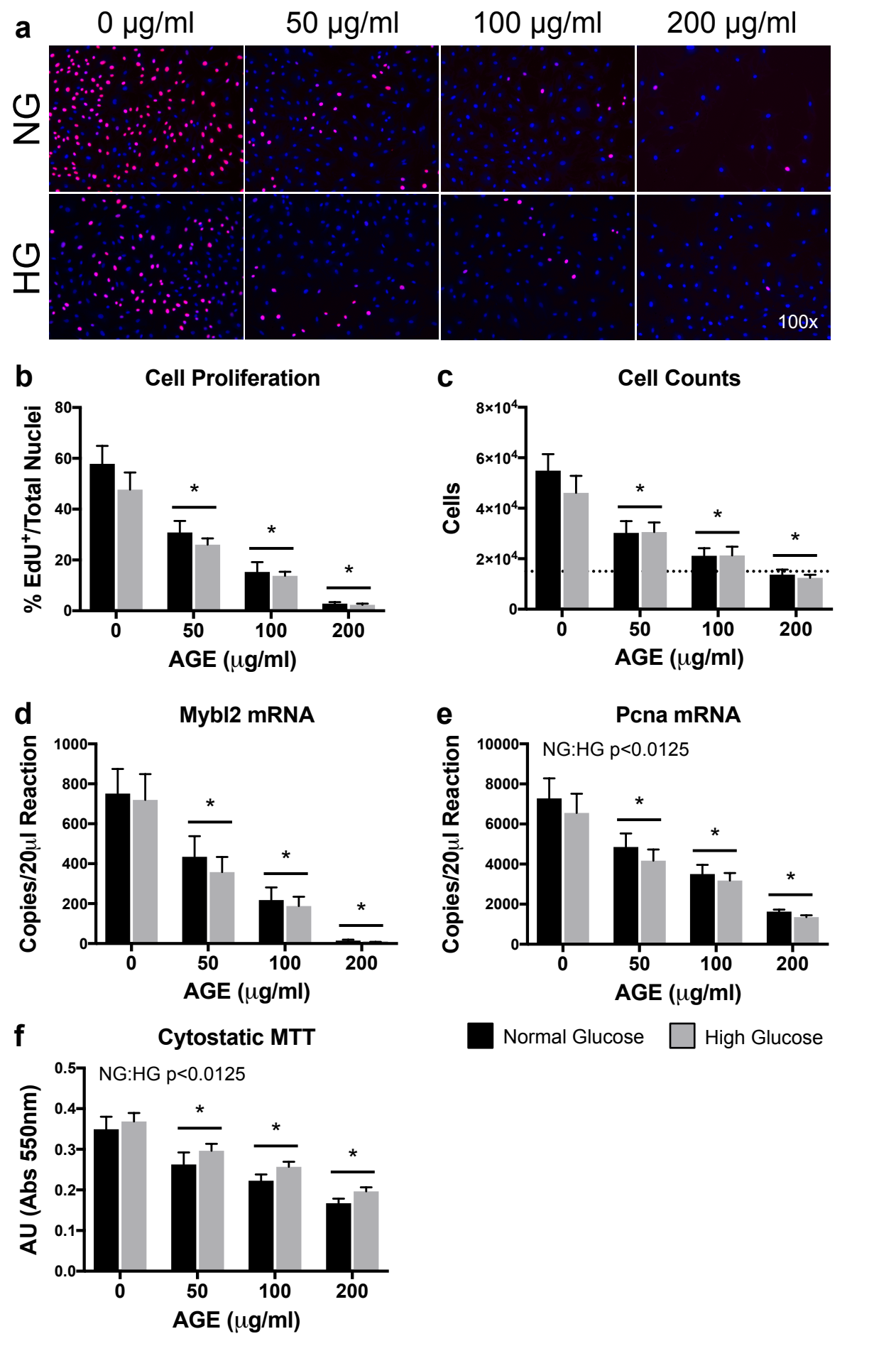
a
0 µg/ml
50 µg/ml
100 µg/ml
200 µg/ml
NG
HG
100x
b
Cell Proliferation
% EdU+/Total Nuclei
AGE (µg/ml)
c
Cell Counts
Cells
AGE (µg/ml)
d
Mybl2 mRNA
Copies/20µl Reaction
AGE (µg/ml)
e
Pcna mRNA
NG:HG p<0.0125
Copies/20µl Reaction
AGE (µg/ml)
Normal Glucose
High Glucose
f
Cytostatic MTT
NG:HG p<0.0125
AU (Abs 550nm)
AGE (µg/ml)

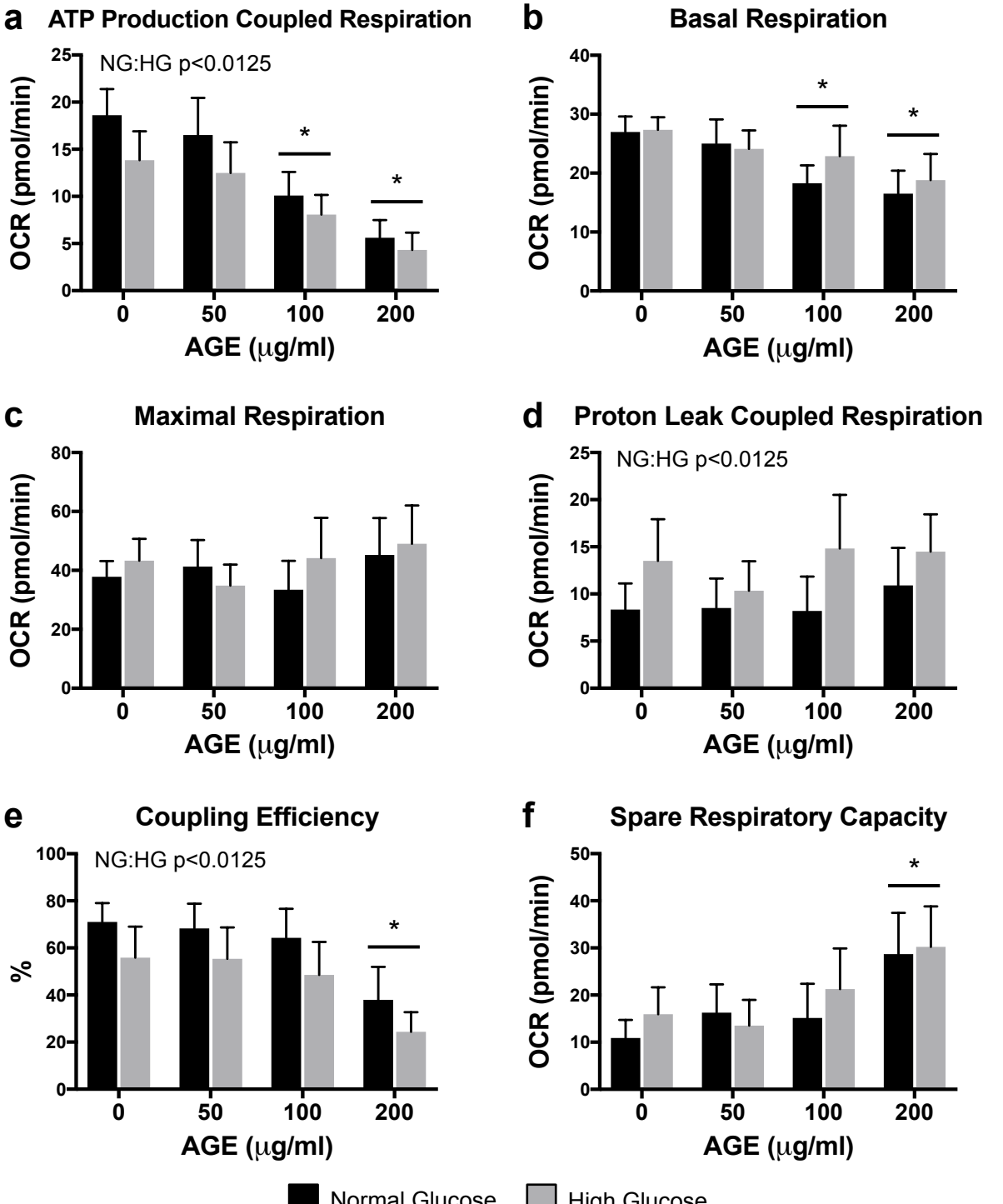
a
ATP Production Coupled Respiration
NG:HG p<0.0125
OCR (pmol/min)
AGE (μg/ml)
b
Basal Respiration
c
Maximal Respiration
d
Proton Leak Coupled Respiration
e
Coupling Efficiency
%
f
Spare Respiratory Capacity
Normal Glucose
High Glucose

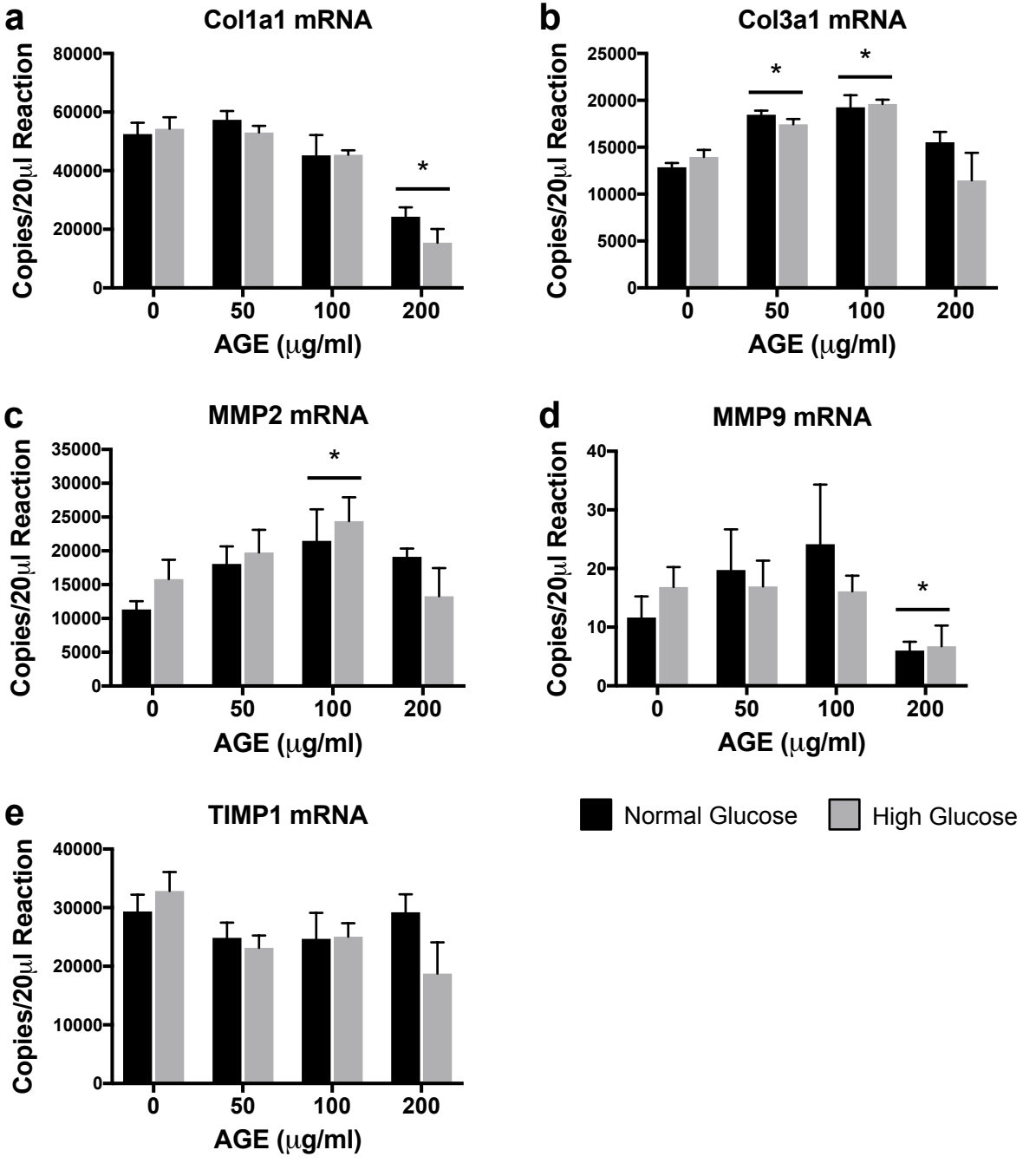
a
Col1a1 mRNA
Copies/20μl Reaction
80000
60000
40000
20000
0
*
0
50
100
200
AGE (μg/ml)
b
Col3a1 mRNA
Copies/20μl Reaction
25000
20000
15000
10000
5000
0
*
*
0
50
100
200
AGE (μg/ml)
c
MMP2 mRNA
Copies/20μl Reaction
35000
30000
25000
20000
15000
10000
5000
0
*
0
50
100
200
AGE (μg/ml)
d
MMP9 mRNA
Copies/20μl Reaction
40
30
20
10
0
*
0
50
100
200
AGE (μg/ml)
e
TIMP1 mRNA
Copies/20μl Reaction
40000
30000
20000
10000
0
0
50
100
200
AGE (μg/ml)
Normal Glucose
High Glucose

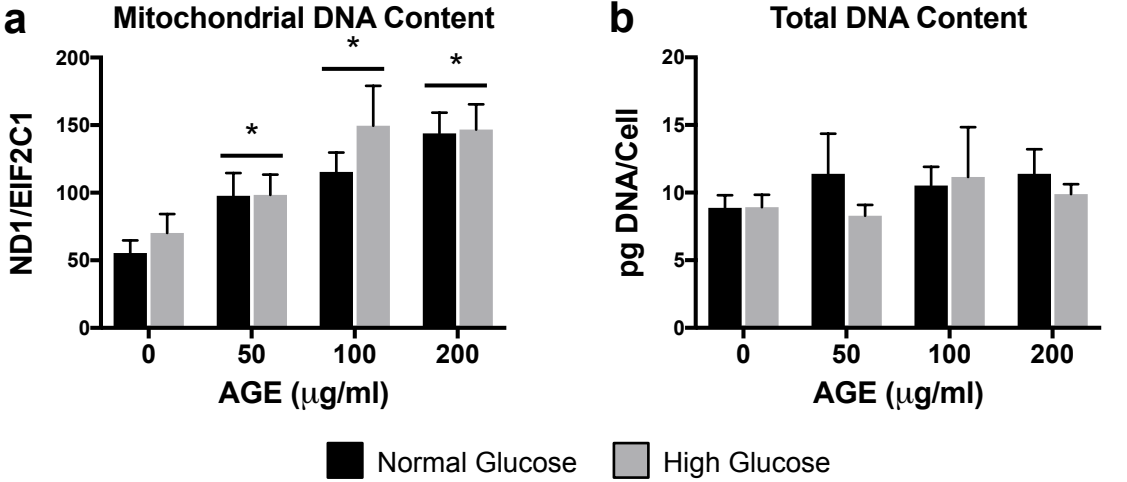
a
Mitochondrial DNA Content
ND1/EIF2C1
200
150
100
50
0
*
*
*
0
50
100
200
AGE (μg/ml)
b
Total DNA Content
pg DNA/Cell
20
15
10
5
0
0
50
100
200
AGE (μg/ml)
Normal Glucose
High Glucose

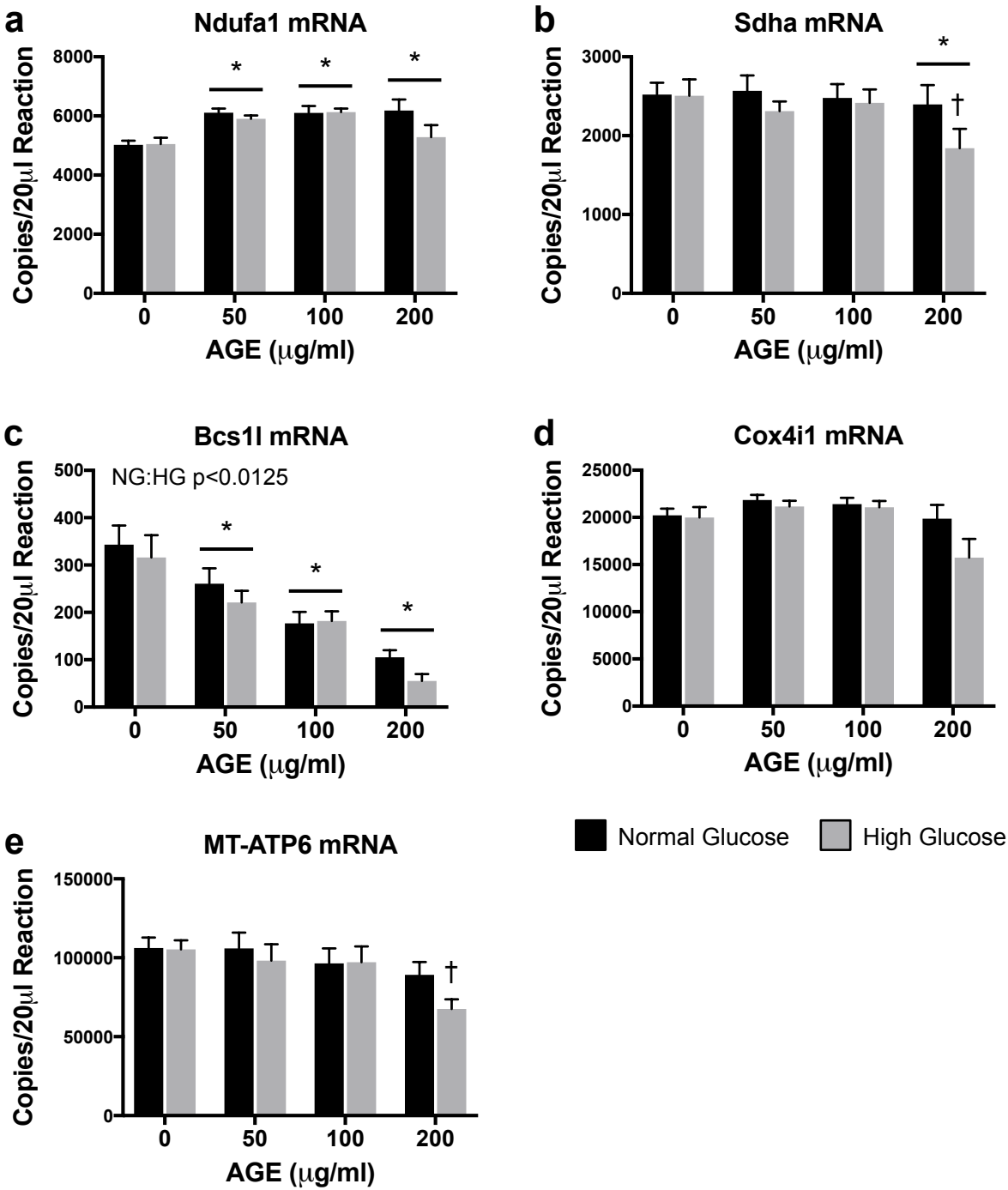
a
Ndufa1 mRNA
Copies/20μl Reaction
8000
6000
4000
2000
0
*
*
*
0
50
100
200
AGE (μg/ml)
b
Sdha mRNA
Copies/20μl Reaction
3000
2000
1000
0
*
†
0
50
100
200
AGE (μg/ml)
c
Bcs1l mRNA
NG:HG p<0.0125
Copies/20μl Reaction
500
400
300
200
100
0
*
*
*
0
50
100
200
AGE (μg/ml)
d
Cox4i1 mRNA
Copies/20μl Reaction
25000
20000
15000
10000
5000
0
0
50
100
200
AGE (μg/ml)
Normal Glucose
High Glucose
e
MT-ATP6 mRNA
Copies/20μl Reaction
150000
100000
50000
0
†
0
50
100
200
AGE (μg/ml)

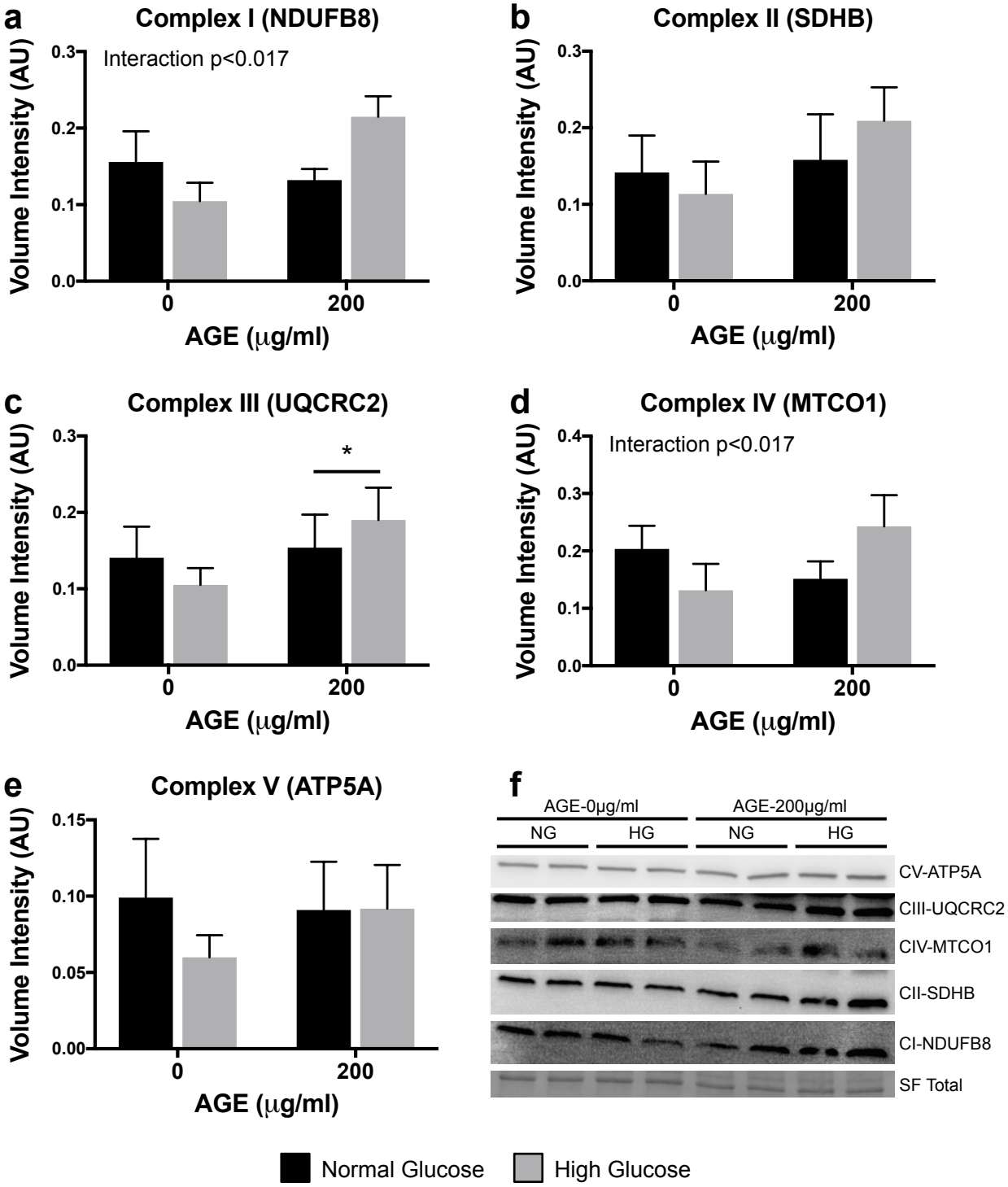
a
Complex I (NDUFB8)
Interaction p<0.017
Volume Intensity (AU)
0.3
0.2
0.1
0.0
0
200
AGE (μg/ml)
b
Complex II (SDHB)
Volume Intensity (AU)
0.3
0.2
0.1
0.0
0
200
AGE (μg/ml)
c
Complex III (UQCRC2)
*
Volume Intensity (AU)
0.3
0.2
0.1
0.0
0
200
AGE (μg/ml)
d
Complex IV (MTCO1)
Interaction p<0.017
Volume Intensity (AU)
0.4
0.3
0.2
0.1
0.0
0
200
AGE (μg/ml)
e
Complex V (ATP5A)
Volume Intensity (AU)
0.15
0.10
0.05
0.00
0
200
AGE (μg/ml)
f
AGE-0μg/ml
AGE-200μg/ml
NG
HG
NG
HG
CV-ATP5A
CIII-UQCRC2
CIV-MTCO1
CII-SDHB
CI-NDUFB8
SF Total
Normal Glucose
High Glucose

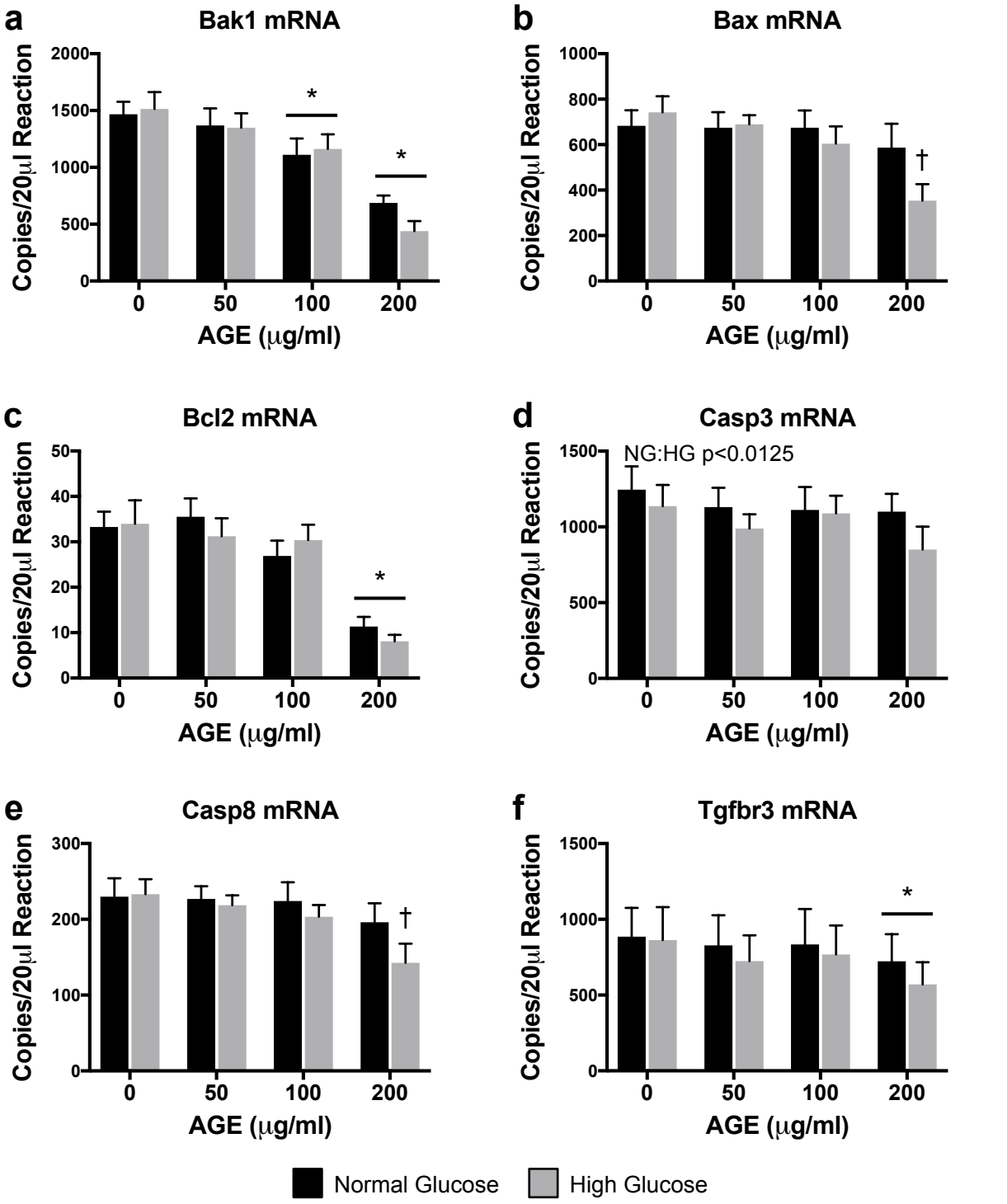
a
Bak1 mRNA
Copies/20μl Reaction
2000
1500
1000
500
0
*
*
0
50
100
200
AGE (μg/ml)
b
Bax mRNA
Copies/20μl Reaction
1000
800
600
400
200
0
†
0
50
100
200
AGE (μg/ml)
c
Bcl2 mRNA
Copies/20μl Reaction
50
40
30
20
10
0
*
0
50
100
200
AGE (μg/ml)
d
Casp3 mRNA
NG:HG p<0.0125
Copies/20μl Reaction
1500
1000
500
0
0
50
100
200
AGE (μg/ml)
e
Casp8 mRNA
Copies/20μl Reaction
300
200
100
0
†
0
50
100
200
AGE (μg/ml)
f
Tgfbr3 mRNA
Copies/20μl Reaction
1500
1000
500
0
*
0
50
100
200
AGE (μg/ml)
Normal Glucose
High Glucose

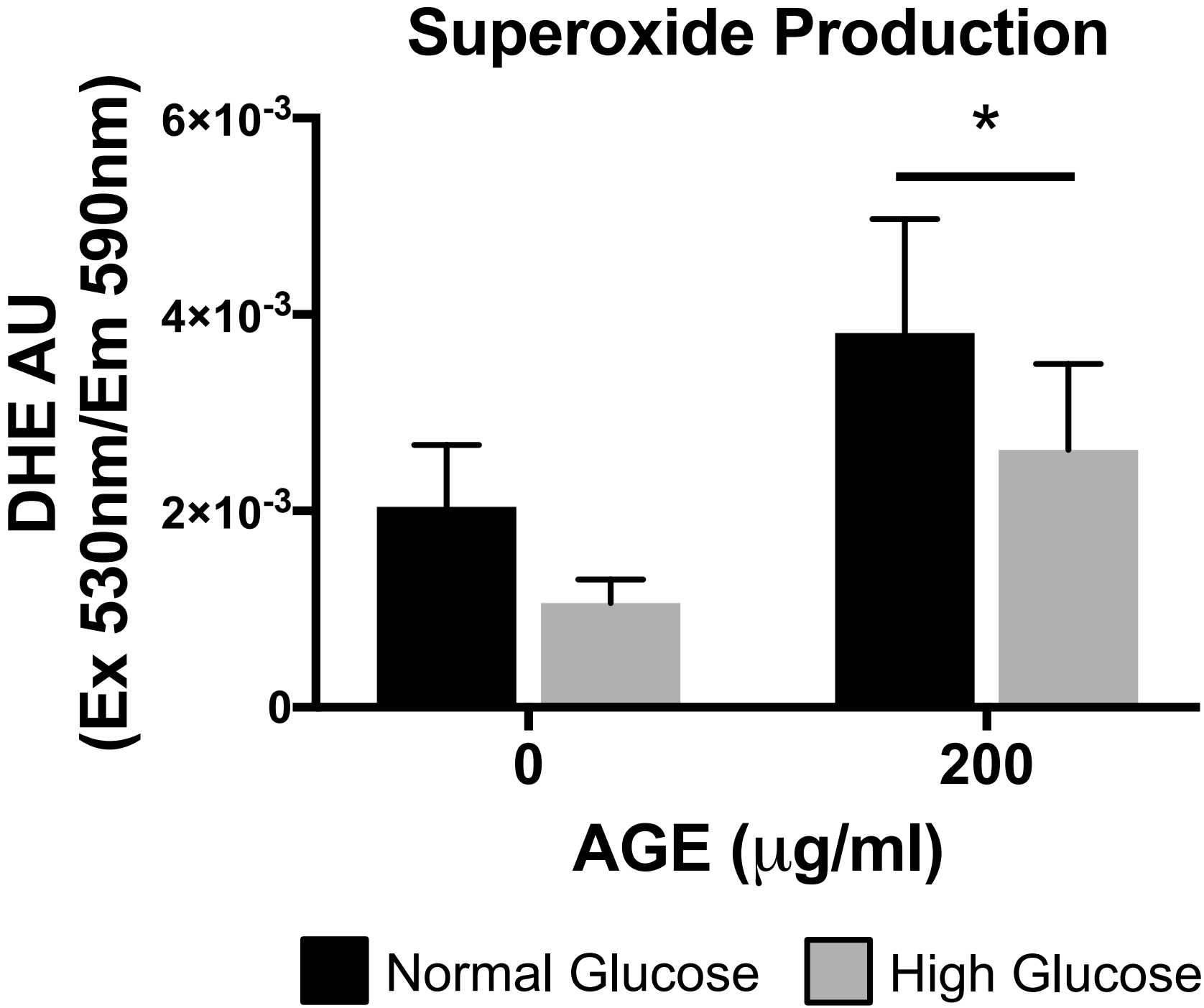
Superoxide Production
DHE AU
(Ex 530nm/Em 590nm)
6×10-3
4×10-3
2×10-3
0
*
0
200
AGE (μg/ml)
Normal Glucose
High Glucose

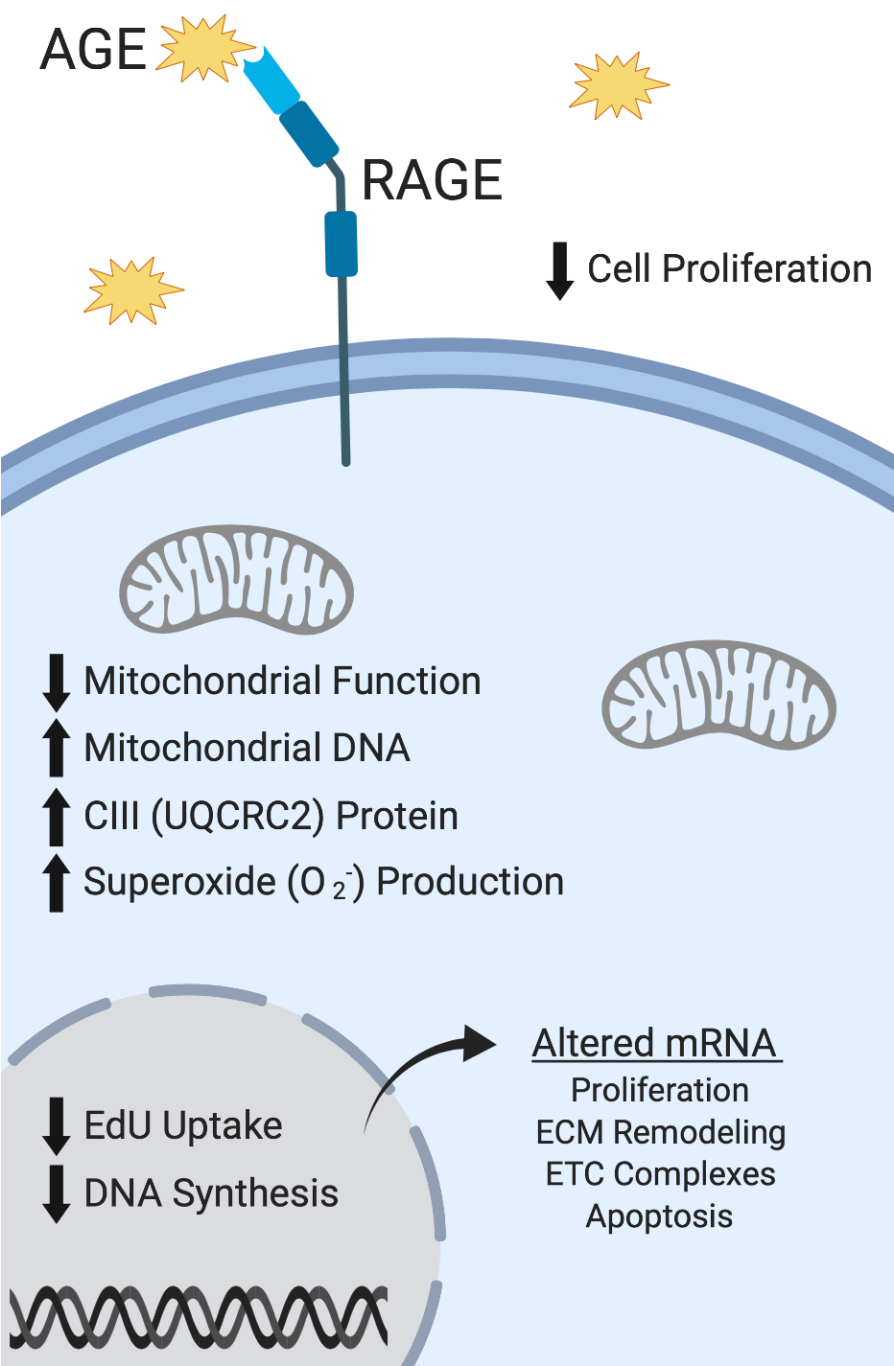
AGE
RAGE
Cell Proliferation
Mitochondrial Function
Mitochondrial DNA
CIII (UQCRC2) Protein
Superoxide (O_2^-) Production
EdU Uptake
DNA Synthesis
Altered mRNA
Proliferation
ECM Remodeling
ETC Complexes
Apoptosis